3D RECONSTRUCTION OF POINT-LIKE SOURCES IN A J-PET SCANNER USING TOTAL VARIATION REGULARIZATION*

L. Raczyński

on behalf of the J-PET Collaboration

Department of Complex Systems, National Centre for Nuclear Research
05-400 Otwock-Świerk, Poland

(Received November 25, 2019)

In this paper, we provide a comparative study of two image reconstruction algorithms for positron emission tomography (PET): a novel reconstruction method based on the concept of total variation (TV) regularization and a reference Time-Of-Flight filtered back-projection (TOF-FBP) technique. The methods are validated using experimental data of the Jagiellonian-PET (J-PET) scanner from measurement of six point-like sources. The spatial resolution of the J-PET scanner was determined by estimation of the full width half maximum in transverse and longitudinal directions of the point spread function at six positions inside the scanner volume. The comparison results show a superior spatial resolution of reconstructed images from the proposed TV-based method with respect to the TOF-FBP algorithm. Simultaneously, reconstruction time of the proposed technique was approximately 2.2 times shorter than required by the TOF-FBP method.

DOI:10.5506/APhysPolB.51.175

1. Introduction

Time-Of-Flight (TOF) PET systems were first developed in the early 1980s [1, 2] and until recently had a timing resolution of a few nanoseconds. The introduction of fast scintillation crystals, such as LSO [3], revitalized TOF as an area of interest. The best present TOF-PET systems based on silicon photomulipliers (SiPM) detectors achieve timing resolution of around 200–300 ps [4, 5]. To improve timing resolution, increase the geometrical acceptance and introduce positronium imaging [6, 7], the Jagiellonian PET (J-PET) Collaboration developed a novel system based on plastic scintillators [8–12].

* Presented at the 3rd Jagiellonian Symposium on Fundamental and Applied Subatomic Physics, Kraków, Poland, June 23–28, 2019.

The recent results [13] suggest that as the timing resolution improves, the TOF analytic algorithms, *e.g.*, TOF filtered back-projection (TOF-FBP), become more competitive to iterative methods. However, analytic algorithms exhibit higher sensitivity to the data noise, as compared to the statistical iterative approaches. Consequently, proper regularization of the analytic reconstruction is of a very practical interest.

Key component of this work is the application of the total variation (TV) regularization [14] in the image space during the analytic reconstruction filtering step, that is, after the TOF data have been TOF back-projected into the image space. Image space is substantially reduced in size as compared to the TOF data space, making the TV optimization operations much more efficient. We compare the performance of the proposed TV-based approach with a standard TOF-FBP [15] method using experimental data of the J-PET scanner from measurement of six point-like sources.

2. Materials and methods

This section describes briefly the subsequent steps of the proposed TOF algorithm. As required for analytic reconstruction, in the first step, the TOF events are pre-corrected. Pre-correction considers both the multiplicative factors (detector efficiency and attenuation factors) and the additive contamination of the data (random and scatter events). More details about the pre-correction and pre-processing of the J-PET data may be found in [16, 17].

The corrected data are deposited directly into TOF back-projected image b. The relation between image b and the unknown original radioactive tracer distribution, denoted hereafter with f, is given with the linear system of equations

$$b(\vec{x}\,) = \mathcal{A} f(\vec{x}\,)\,, \tag{1}$$

where $\vec{x} \in \mathbb{R}^3$ denotes the space coordinate, $\mathcal{A}$ is an overall TOF forward- and back-projection operator. The problem in Eq. (1) may be rewritten in the matrix notation

$$\boldsymbol{b} = A\boldsymbol{f}\,, \tag{2}$$

where A is finite-dimensional sampling of operator $\mathcal{A}$ and bold symbols $\boldsymbol{f}$ and $\boldsymbol{b}$ represent the vectorized versions of the functions f and b, respectively. The images $\boldsymbol{f}$ and $\boldsymbol{b}$ have the same sizes and one-to-one voxel correspondence. Since the TOF back-projected image $\boldsymbol{b}$ is not a perfect noiseless image, the filtering problem defined in Eq. (2) is ill-posed. Therefore, the regularization methods are required in order to calculate a meaningful solution. The most common class of regularization methods in the image processing is based on

the TV approach [18]. The TV norm of image $\boldsymbol{f}$ can be defined as

$$\mathrm{TV}(\boldsymbol{f}) = \sum_i |D_i \boldsymbol{f}|\,, \tag{3}$$

where D is a total first-order forward finite-difference operator and $D_i \boldsymbol{f} \in \mathbb{R}^3$ is a discrete gradient of the image at pixel i. Optimization algorithm finds a solution of Eq. (2) by solving an unconstrained regularization problem

$$\min_{\boldsymbol{f}} \ \mathrm{TV}(\boldsymbol{f}) + \frac{\mu}{2}\|A\boldsymbol{f} - \boldsymbol{b}\|_2^2\,, \tag{4}$$

where μ is the regularization parameter. The theory for penalty functions implies that the solution in Eq. (4) approaches the solution of Eq. (2) as μ approaches infinity. The proposed algorithm is based on the augmented Lagrangian method [19]. This algorithm will be denoted hereafter as TOF-BPTV (TOF Back Projection Total Variation Regularization Method).

3. Results

For the evaluation of the proposed image reconstruction approach, an experimental data of the J-PET scanner from measurement of six point-like sources was used. The J-PET detector consists of three concentric cylindrical layers of 192 axially arranged detection modules of plastic scintillator as shown in Fig. 1. Each scintillator strip is 50 cm long with a rectangular cross section of 0.7×1.9 cm^2. Within a detection module, both ends of the scintillator strip are optically coupled to photomultiplier tubes.

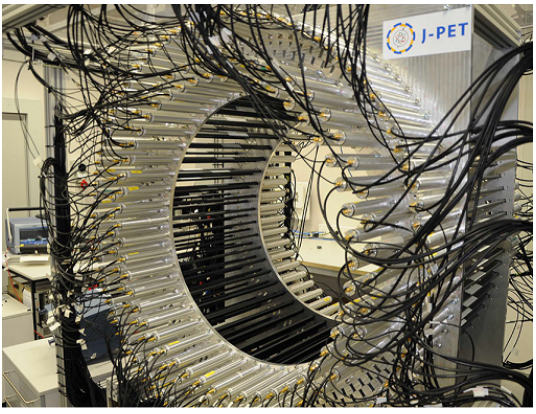

Fig. 1. A photo of the J-PET detector consisting of 192 plastic scintillator strips arranged in three concentric layers.

Measurements were performed with six point-like sources of ^{22}Na placed in positions suggested in the NEMA-NU-2-2012 norm [20]. While in the norm, it is suggested to measure the source subsequently in each positions, in the experiment, six point-like sources with different activities were measured at the same time. Sources were placed at the following positions: $(0, 1, 0)$, $(0, 10, 0)$, $(0, 20, 0)$, $(0, 1, -18.75)$, $(0, 10, -18.75)$ and $(0, 20, -18.75)$. A dedicated styrofoam panel was prepared for measurements; the sources were attached to the panel using an adhesive tape. Styrofoam was chosen because of its low density and small probability for scattering and attenuation on the panel. For this study, a total of 70 million coincident events were recorded, including about 11.2 million events retrieved after data pre-correction and pre-processing according to [16]. During the reconstruction, only those coincidences were taken into consideration. The reconstructed images were 3-dimensional (3D) matrices with the voxel size of $0.4 \times 0.4 \times 0.4$ cm^3.

The spatial resolution of the J-PET scanner was determined by estimation of the full width half maximum in all three directions of Point Spread Function (PSF) at six positions inside the scanner volume. At each position of the reconstructed image, a voxel with the maximum intensity was found and three 1D profiles along each directions (x, y, z) were determined. The two image reconstruction examples, based on proposed TOF-BPTV method and the standard TOF-FBP algorithm with regularization via apodizing functions are shown in Fig. 2 on the right and left panels, respectively. The images were obtained for optimal regularization parameters for both methods, *i.e.*, for parameters that minimize the spatial resolution. For clarity of presentation, the activities of six sources in Fig. 2 were normalized to 1.

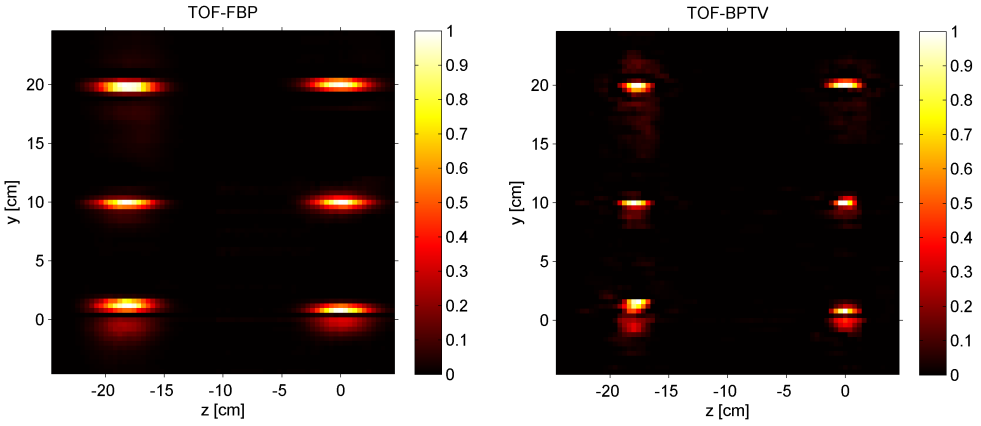

Fig. 2. Images reconstructed with the TOF-FBP algorithm (left) and the proposed TOF-BPTV method (right).

The estimated PSF values for 3D reconstruction of point-sources located in six positions for both methods: TOF-FBP (gray/red solid and dotted line) and TOF-BPTV (black/blue solid and dotted line) are presented in Fig. 3. It may be seen that the TOF-BPTV algorithm achieved slightly better PSF values in transverse direction (see Fig. 3, left panel), resulting in effective spatial resolution of $\sim 0.5 \div 0.8$ cm; PSF values provided by the TOF-FBP method are $\sim 0.7 \div 1.0$ cm. On the other hand, the estimated longitudinal resolution differs significantly for both methods (see Fig. 3, right panel). In this case, the TOF-BPTV algorithm provides almost two-fold reduction in the PSF values compared to the TOF-FBP method.

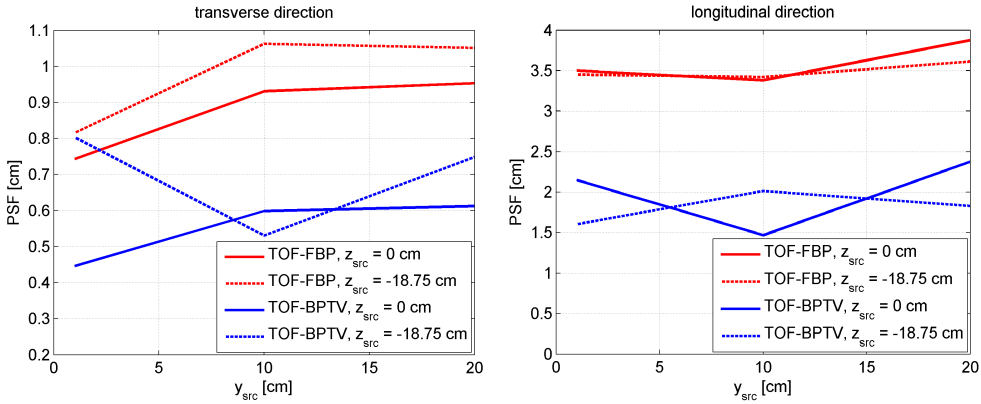

Fig. 3. (Color online) Estimation of PSF values in transverse (left) and longitudinal (right) direction for 3D reconstruction of point source in the J-PET scanner.

In the last part of this study, the computational speed of both reconstruction methods was compared. The reconstruction volume was $50 \times 50 \times 50$ cm^3, comprised of $125 \times 125 \times 125$ voxels. On a single CPU (Intel Core i5-5200U at 2.20 GHz), the total computing time of the TOF-BPTV algorithm for 11.2 million events was 200 s. On the same CPU, the total computing time of the TOF-FBP algorithm was 450 s. Hence, reconstruction time in the TOF-BPTV method was approximately 2.2 times shorter than required by the TOF-FBP reconstruction.

4. Conclusions

In this paper, a novel scheme of regularization in PET image reconstruction, based on the TV method, was introduced. The algorithm takes advantage of the TOF information and the reconstruction problem is formulated entirely in the image space making the TV optimization operations much more efficient. The experimental study with the J-PET data demonstrated

that reconstruction time of the TV-based algorithm was approximately 2.2 times shorter than required by the TOF-FBP reconstruction. Simultaneously, it was shown that the proposed reconstruction method can reach superior spatial resolution of reconstructed images.

We acknowledge support by the Foundation for Polish Science through MPD and TEAM POIR.04.04.00-00-4204/17 programmes, the National Science Centre, Poland (NCN) through the grant No. 2016/21/B/ST2/01222, the Polish Ministry for Science and Higher Education through grant No. 7150/E-338/SPUB/2017/1, the EU and MSHE grant No. POIG.02.03.00-161 00-013/09.

REFERENCES

[1] T. Tomitani, *IEEE Trans. Nucl. Sci.* **28**, 4581 (1981).
[2] D.L. Snyder, D.G. Politte, *IEEE Trans. Nucl. Sci.* **30**, 1843 (1983).
[3] W. Moses, S. Derenzo, *IEEE Trans. Nucl. Sci.* **46**, 474 (1999).
[4] P. Słomka *et al.*, *Semin. Nucl. Med.* **46**, 5 (2016).
[5] J. van Sluis *et al.*, *J. Nucl. Med.* **60**, 1031 (2019).
[6] P. Moskal *et al.*, *Phys. Med. Biol.* **64**, 055017 (2019).
[7] P. Moskal, B. Jasińska, E. Stepień, S. Bass, *Nature Phys. Rev.* **1**, 527 (2019).
[8] P. Moskal *et al.*, *Nucl. Instrum. Methods Phys. Res. A* **764**, 317 (2014).
[9] P. Moskal *et al.*, *Phys. Med. Biol.* **61**, 2025 (2016).
[10] L. Raczyński *et al.*, *Nucl. Instrum. Methods Phys. Res. A* **786**, 105 (2015).
[11] G. Korcyl *et al.*, *IEEE Trans. Med. Imaging* **37**, 2526 (2018).
[12] P. Kowalski *et al.*, *Phys. Med. Biol.* **63**, 165008 (2018).
[13] V. Westerwoudt *et al.*, *IEEE Trans. Nucl. Sci.* **61**, 126 (2014).
[14] L. Rudin *et al.*, *Physica D* **60**, 259 (1992).
[15] M. Conti *et al.*, *Phys. Med. Biol.* **50**, 4507 (2005).
[16] M. Pawlik-Niedźwiecka *et al.*, *Acta Phys. Pol. A* **132**, 1645 (2017).
[17] S. Niedźwiecki *et al.*, *Acta Phys. Pol. B* **48**, 1567 (2017).
[18] P. Blomgren *et al.*, *IEEE Trans. Image Process.* **7**, 304 (1998).
[19] S. Chan *et al.*, *IEEE Trans. Image Process.* **20**, 3097 (2011).
[20] National Electrical Manufacturers Association, Norm NEMA-NU-2 Performance Measurements of Positron Emission Tomographs (PETs), 2012.